International Journal of Disaster Risk Science (2026) 17:182–196
https://doi.org/10.1007/s13753-026-00697-y

www.ijdrs.com
www.springer.com/13753

ARTICLE

A Dynamic Simulation Framework for Evaluating the Impacts of Urban Flooding on Transportation Systems

Jiayue Li[1,2,3] · Zhiwei Chen[1,2] · Guoru Huang[1,2] · Guangtao Fu[3]

Accepted: 21 December 2025 / Published online: 10 February 2026

Abstract
Road networks are a critical infrastructure system for the sustainable functioning of cities. However, they are frequently disrupted by urban flooding, leading to increased travel times and hindering emergency responses. This study proposed a novel dynamic flood–response simulation framework for urban transportation to evaluate the impacts of rainstorms and flooding on traffic systems, focusing on coupling the Integrated Hydrology and Hydrodynamics Urban Flood Model (IHUM) and the Simulation of Urban MObility (SUMO) model. The results obtained from Xiaoguwei Island, Guangzhou City, indicate that a 2-h rainstorm of a 2-year return period can affect traffic for over 4.5 h. During a 100-year return period rainstorm, average travel speed declines by 54%, while the emergency response time, for example, for police services, increases from 4.83 to 14.52 min. These findings highlight the significant impacts of flooding on urban traffic networks, assisting local authorities and stakeholders to proactively identify vulnerable network segments and prioritize targeted interventions for enhancing transportation system resilience to floods.

Keywords Flood management · Flood modeling · Road traffic · Transportation modeling · Urban resilience

1 Introduction

The potential impacts of climate change and urbanization require urban inhabitants to prepare for an increasing frequency of disasters, such as heatwaves and flooding (de Abreu et al. 2022; Lu et al. 2022; Rentschler et al. 2022). Urban road networks, as part of the critical infrastructure, are particularly vulnerable to flooding (Singh et al. 2018; Zheng and Huang 2023). Flooding of road networks may result in a heightened incidence of vehicle malfunctions, collisions, and fatalities, which have been escalating in severity and attracting growing public concern (Martínez-Gomariz et al. 2018; Ahmed et al. 2020a; Tobin et al. 2021; Zou et al. 2021).

✉ Guoru Huang
huanggr@scut.edu.cn

[1] State Key Laboratory of Subtropical Building and Urban Science, South China University of Technology, Guangzhou 510640, China

[2] School of Civil Engineering and Transportation, South China University of Technology, Guangzhou 510640, China

[3] Centre for Water Systems, University of Exeter, Exeter EX4 4QF, UK

Previous research has investigated the impacts of rainstorms and flooding on urban transportation from various perspectives. Generally, intense precipitation primarily affects driving behavior by influencing visibility and inundation (Su et al. 2016; Phanse et al. 2022). Due to safety considerations, drivers tend to reduce speed, resulting in a lower overall flow rate in the traffic system (Hamzeie et al. 2017). Furthermore, drivers are likely to brake more frequently in stormy conditions, which leads to speed fluctuations, ultimately causing significant congestion or potential traffic accidents (Li et al. 2018; Markolf et al. 2019; Wang et al. 2019; He et al. 2023). Suarez et al. (2005) incorporated future climate change predictions into urban transportation system modeling, suggesting that flooding and climate change will double travel delays. Resident commuting is a significant aspect of urban travel. Therefore, incorporating it into the evaluation of flooding impacts on traffic facilitates a more thorough understanding of the interplay between the physical and social attributes of cities (Lutoff et al. 2018; Li et al. 2019; Zhu et al. 2019; Tang et al. 2023). Debionne et al. (2016) discovered that daily mobility amplifies flood risk, and commuters with longer routes are more susceptible to flooding in the Gard Region, France. Along with residential commuters, emergency response vehicles are

a significant part of traffic. During rainstorms, when the accessibility of emergency vehicles, such as fire engines and ambulances, is compromised, cities face more threats (Chakraborty et al. 2018; Fan et al. 2022; Miller 2022).

An integrated flood–traffic analysis is essential for assessing the impacts of flooding on traffic networks. Currently, two approaches are commonly adopted. The first approach is a comprehensive physics-based modeling strategy. For example, Pyatkova et al. (2019) used MIKE FLOOD, an established commercial flood model, together with Simulation of Urban MObility (SUMO) (Krajzewicz 2010; Lopez et al. 2018), an open-source, microscopic, multimodal traffic simulation model, to conduct integrated analyses and demonstrate the impairment of traffic networks during precipitation events. The second approach involves simplified physics-based or data-driven analytical strategies. For instance, Li et al. (2019) applied a cellular automata model to simulate dynamic flooding processes in urban environments, integrating urban commuter characteristics into the grid using correlation equations to evaluate the impacts of flooding on road networks. Wang et al. (2020) simulated future flood scenarios using the CaMa-Flood model and assessed vehicle behavior in a flood-impacted highway network through a multi-agent simulation model. Fan et al. (2021) proposed an adaptive reinforcement learning model that leveraged extensive trajectory data to learn travel patterns and simulated changes in travel routes during flooding events, providing insights into the effects of flooding on urban transportation systems.

Compared to simplified physics-based or data-driven analytical strategies, a comprehensive physics-based modeling strategy is better in high-precision dynamic analysis. The former approach demonstrates adaptability to diverse scenarios and facilitates rapid modeling, providing higher flexibility and faster results. However, the lack of specific physical constraints can lead to instability and unreliability under complex or extreme conditions. The latter approach excels at accurately capturing flood dynamics and traffic alteration, yielding reliable quantitative analysis results, and enabling capabilities for a thorough evaluation of flood impacts on transportation systems.

At the current stage, the use of a comprehensive physics-based modeling strategy for integrated flood and traffic analysis remains limited. Early studies attempted to statically combine flood maps with transportation systems (Suarez et al. 2005). Later research introduced flood estimation or macroscopic traffic simulations (Chang et al. 2010; Borowska-Stefańska et al. 2019; Vajjarapu et al. 2020). More recently, dynamic integration of flood and traffic models has provided better guidance for evaluating the impacts of flooding on transportation networks (Pyatkova et al. 2019; Shahdani et al. 2022). However, in these studies, vehicle speeds under different inundation conditions are often depicted using a fixed speed-reduction ratio or by giving a low value. Such methods lack empirical restrictions on vehicular behavior in flooding conditions, resulting in a loose integration between the flood and traffic components and failing to reflect the systematic variation of vehicle speed with water depth. At the same time, modeling the mobility of emergency vehicles, such as ambulances and fire engines, is crucial during disaster management, yet this aspect has received little attention in coupled flood–traffic studies.

In this study, we proposed a novel dynamic flood–response simulation framework for urban transportation, grounded in a comprehensive physics-based modeling strategy. The framework incorporates an in-house Integrated Hydrology and Hydrodynamics Urban Flood Model (IHUM) (Chen et al. 2018; Li, Zeng, et al. 2024) with the SUMO model, developed by the German Aerospace Center (Krajzewicz 2010). The integration is achieved using empirically observed relationships between water depth and vehicle speed, enabling an explicit representation of the dynamic linkage between flood and traffic models. In addition, key components such as the drainage network and emergency vehicles are incorporated, allowing the framework not only to capture street-level flood and traffic dynamics but also to provide routing recommendations for emergency vehicles during rainstorms.

2 Methodology

Figure 1 illustrates the dynamic flood–response simulation framework for urban transportation. First, the flood model IHUM is constructed using a two-layer drainage system concept, which considers both the underground drainage network and the surface drainage system. Second, the traffic model SUMO is established based on road network topology and residential travel demand. Finally, we connect the flood model and the traffic model using the relationship between water depth and vehicle speed. The framework takes rainstorm data as input and, following the flood–traffic dual-model processing, generates lane-level vehicle information, including speed, duration, trajectories, and additional statistics, which is capable of illustrating the impacts of flooding on road traffic.

2.1 Study Area

Xiaoguwei Island, which is the location of Guangzhou University Town, was selected as the study area. It covers an area of approximately 18 km^2, has a population of around 233,000, and receives an average annual precipitation of 1923 mm. Located in a subtropical monsoon climate zone, Xiaoguwei Island exhibits strong oceanic climate characteristics and is prone to typhoons, rainstorms, and flooding.

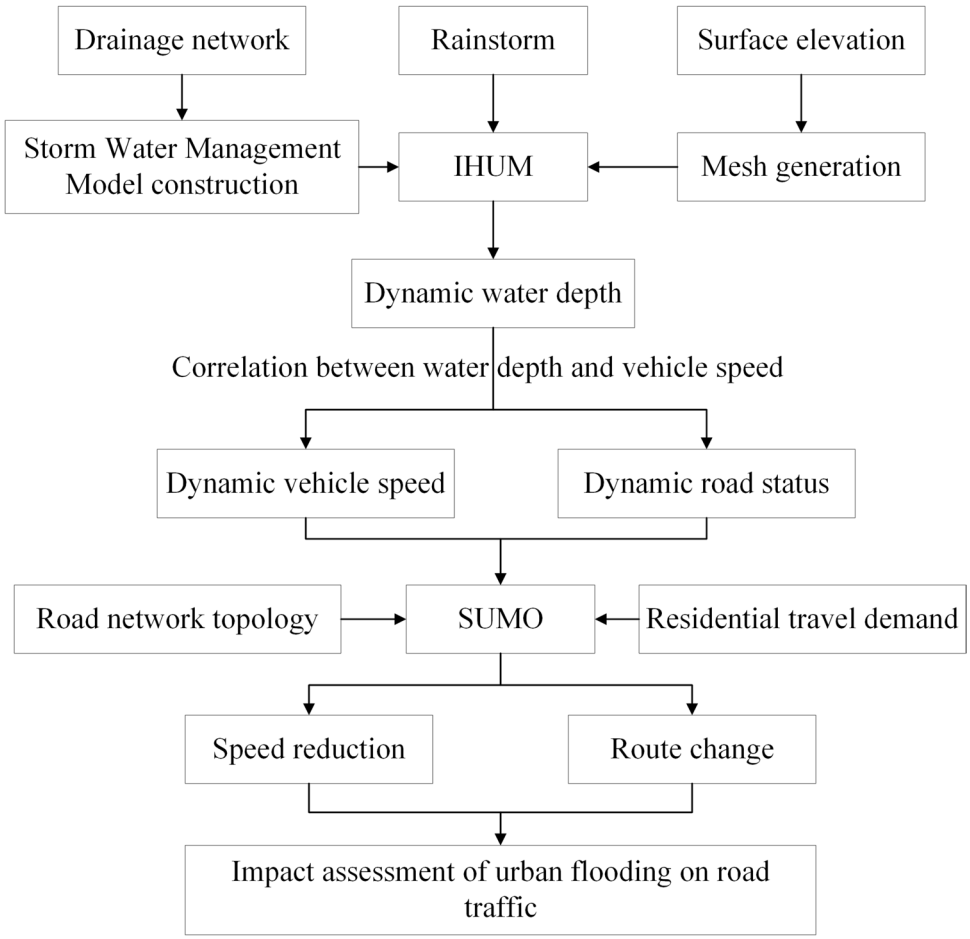

Fig. 1 A dynamic flood–response simulation framework for urban transportation. *IHUM* Integrated Hydrology and Hydrodynamics Urban Flood Model, *SUMO* Simulation of Urban MObility

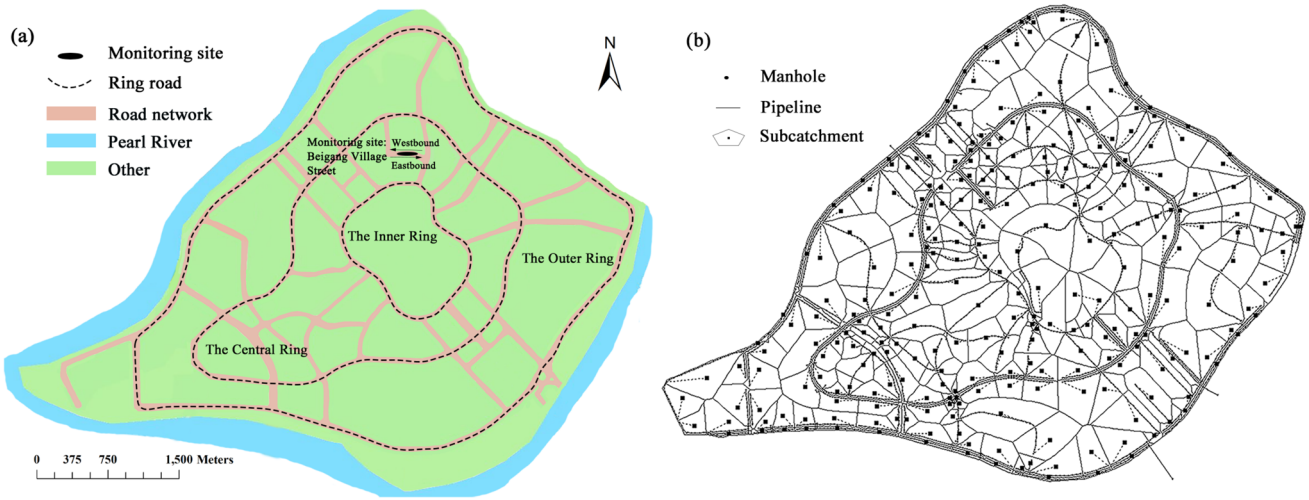

Fig. 2 Xiaoguwei Island. **a** The main road network, and **b** Storm Water Management Model (SWMM) for the study area

The island's transportation system is structured around three ring roads: the Inner Ring, the Central Ring, and the Outer Ring (Fig. 2a). Most commuters are staff and students from 10 universities, along with residents from four reserved villages.

We used the following rainstorm intensity formula specific to Panyu District of Guangzhou City, where the study area is located, to design the rainstorm scenarios:

$$q = 2458.657(1 + 0.476 \ln P)/(t + 8.873)^{0.749}, \quad (1)$$

where q is the design rainstorm intensity; P is the return period; and t is time.

Considering the substantial impact of single-peak rainstorm events on road networks' vulnerability (Zhang et al. 2021), the design rainstorms are assumed to follow the Chicago rainfall pattern. The 2-h rainstorm profiles for different return periods are calculated using the following equations:

$$\text{For rainstorm intensity: } q = S_p/(t + b)^n, \quad (2)$$

$$\text{Pre-peak intensity: } i = S_p/(t/r + b)^n\left[1 - nt_1/\left(t_1 + rb\right)\right], \quad (3)$$

$$\text{Post-peak intensity: } i = S_p/(t/(1 - r) + b)^n\left[1 - nt_2/\left(t_2 + rb\right)\right], \quad (4)$$

where i is instantaneous rainfall intensity; r is peak rainfall coefficient; t_1 and t_2 are pre- and post-peak times in min, respectively; and S_p, n, and b are correlation parameters. The rainstorms with return periods of 2, 5, 10, 20, 50, and 100 years were considered in this study, as shown in Fig. 3.

2.2 Construction of an Integrated Urban Flood Model

This study used the IHUM to simulate flooding on Xiaoguwei Island, which integrates the Storm Water Management Model (SWMM) (Gironás et al. 2010; Jiang et al. 2015) with a two-dimensional (2D) model based on the shallow water equations through a dynamic link library. The SWMM handles calculations related to rainfall and runoff, as well as pipe and river networks. Meanwhile, the 2D model primarily simulates the water flow that overflows from manholes or rivers onto the surface, as well as its backflow into the drainage system when water levels permit. The 2D model employs unstructured meshes and the finite volume method, specifically using an implicit dual-time stepping approach for solving partial differential equations to enhance the model's robustness.

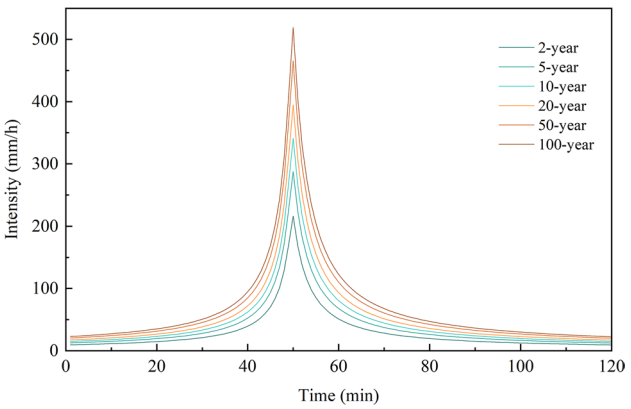

Fig. 3 Design rainstorms with return periods ranging from 2 to 100 years

To obtain accurate information about the pipe network and terrain of the study area, we conducted field research and consulted the local hydrological department. Constructing the SWMM model requires precise details on manholes, drainage pipes, and subcatchment characteristics. Using the acquired pipe network data, we extracted the primary drainage pipelines within the research area and verified the topology in GIS. We analyzed remote sensing imagery of Xiaoguwei Island to classify various land use types and then delineated subcatchments based on roads, buildings, and surface elevation trends (Li, Huang et al. 2024). Figure 2b shows the SWMM model for the study area, which includes 2703 manholes, 2727 pipelines, and 273 subcatchments.

The SWMM model includes several uncertain parameters that require calibration, such as Manning's coefficients for pervious and impervious surfaces, storage depth in depressions, and the parameters related to Horton's infiltration model. Due to difficulties in obtaining measured runoff data, we applied the integrated runoff coefficient method for parameter calibration. This approach involves calculating the theoretical integrated runoff coefficient for the study area, assessing the sensitivity of the uncertain parameters, and adjusting them accordingly to ensure the model-simulated integrated runoff coefficient matches the theoretically calculated value.

Based on the Outdoor Wastewater Engineering Design Standard (GB 50014-2021) and the land use ratio of the study area, we derived a theoretical integrated runoff coefficient of 0.61. The modified Morris screening method (Paleari et al. 2021) (Eq. 5) was used for sensitivity analysis, where the absolute value of M indicates the parameter's sensitivity level.

$$M = \sum_{i=0}^{n-1} \frac{(Y_{i+1} - Y_i)/Y_0}{(P_{i+1} - P_i)/100}/n, \quad (5)$$

where M is sensitivity factor; n is the number of runs; Y_i is integrated runoff coefficient result of the ith run; Y_0 is initial integrated runoff coefficient result; and P_i is percentage change in the parameters used in the ith simulation compared to the initial parameters.

The results of the runoff coefficient sensitivity analysis for each parameter are shown in Table 1. Based on the sensitivity analysis, we adjusted the uncertain parameters in the SWMM, yielding a simulated integrated runoff coefficient of 0.61 for the study area. The final calibrated values of the SWMM parameters for Xiaoguwei Island are listed in Table 2.

Table 1 Sensitivity analysis of Storm Water Management Model (SWMM) parameters

Parameter	Meaning	Runoff coefficient sensitivity factor *M*	Runoff coefficient sensitivity
Zero-imperv	Percent of impervious area with no depression storage (%)	0.02	Non-sensitive
N-imperv	Mannings *N* for impervious area	−0.21	Sensitive
N-perv	Mannings *N* for pervious area	−0.02	Non-sensitive
Dstore-imperv	Depth of depression storage on impervious area (mm)	−0.07	Medium sensitive
Dstore-perv	Depth of depression storage on pervious area (mm)	−0.02	Non-sensitive
MaxRate	Maximum rate on the Horton infiltration curve (mm/h)	−0.04	Non-sensitive
MinRate	Minimum rate on the Horton infiltration curve (mm/h)	0.00	Non-sensitive
Decay Constant	Decay constant for the Horton infiltration curve (1/h)	0.03	Non-sensitive
Drying Time	Time for a fully saturated soil to completely dry (day)	0.00	Non-sensitive

$|M| \geq 1$ is highly sensitive; $|M| \geq 0.2$ is sensitive; $|M| \geq 0.05$ is medium sensitive; $|M| \geq 0$ is non-sensitive

Table 2 Calibrated Storm Water Management Model (SWMM) parameter values for Xiaoguwei Island

Parameter	Value	Parameter	Value
Zero-imperv	50.00	Dstore-perv	3.80
N-imperv	0.01	MaxRate	76.00
N-perv	0.05	MinRate	2.50
Dstore-imperv	1.00	Decay Constant	8.00

The 2D component of the IHUM relies on unstructured meshes, which were generated from the elevation map of Xiaoguwei Island. The meshes were refined along the traffic road to satisfy the analytical accuracy requirements of this study. Meanwhile, buildings were designated as solid wall boundaries, while water bodies were set as open boundaries. Finally, the SWMM file, mesh file, and boundary file were integrated into the IHUM to simulate urban flooding.

2.3 Construction of an Urban Microscopic Traffic Simulation Model

Traffic simulation models are categorized as macroscopic, mesoscopic, or microscopic based on the level of detail used to represent the traffic system. Microscopic models offer sufficient granularity and flexibility in capturing vehicle speed variations, trajectory tracking, and traffic congestion dynamics, making them appropriate for the objectives and requirements of this study. Among the existing microscopic traffic simulation models, the open-source nature of the SUMO model allows researchers to make personalized modifications (Phanse et al. 2022). In this study, SUMO proves advantageous in dynamically adjusting traffic parameters in response to flooding, enabling lane-level speed limit changes and road status control.

The construction of the SUMO model principally involves road network topology and residential travel demand data. The former represents the traffic supply side, while the latter reflects the traffic demand side. The interaction between these two elements determines the actual traffic conditions in the region. When supply exceeds demand, traffic flows smoothly. However, when demand exceeds supply, congestion occurs. On the supply side, a road network topology file for the traffic modeling area was downloaded from the OpenStreetMap website as input for the SUMO model. Compared to real-world conditions, the downloaded road network topology contained inaccuracies, requiring adjustments to lane numbers, turning regulations at intersections, and signal phasing for each road using reference images from Baidu Maps. On the demand side, residential travel demand in the study area is influenced by factors such as population, number of households, unemployment rate, demographic distribution across age groups, commuting time patterns, and the spatial distribution of population and employment along each street. We analyzed relevant socioeconomic data from the area and integrated them with uncertain parameters, including the leisure activity rate and the stochastic flow, to generate comprehensive, activity-based travel demand.

The site visit revealed recurrent congestion on Beigang Village Street, which is located near a major commercial center on Xiaoguwei Island with considerable traffic flow. Thus, we conducted on-site monitoring of the two-way lanes on Beigang Village Street (designated as westbound and eastbound) for three consecutive days, recording vehicle counts every half hour from 11:00 a.m. to 7:00 p.m. daily. These monitoring data were used to calibrate the parameters of the SUMO model. Ultimately, the simulated values closely matched the 3-day monitoring data in both magnitude and trend, as observed from the two directions of Beigang Village Street (Fig. 4).

To evaluate the reliability of the overall SUMO traffic simulation results, we used real-time data from Gaode Maps route planning API, which enables calculating routes

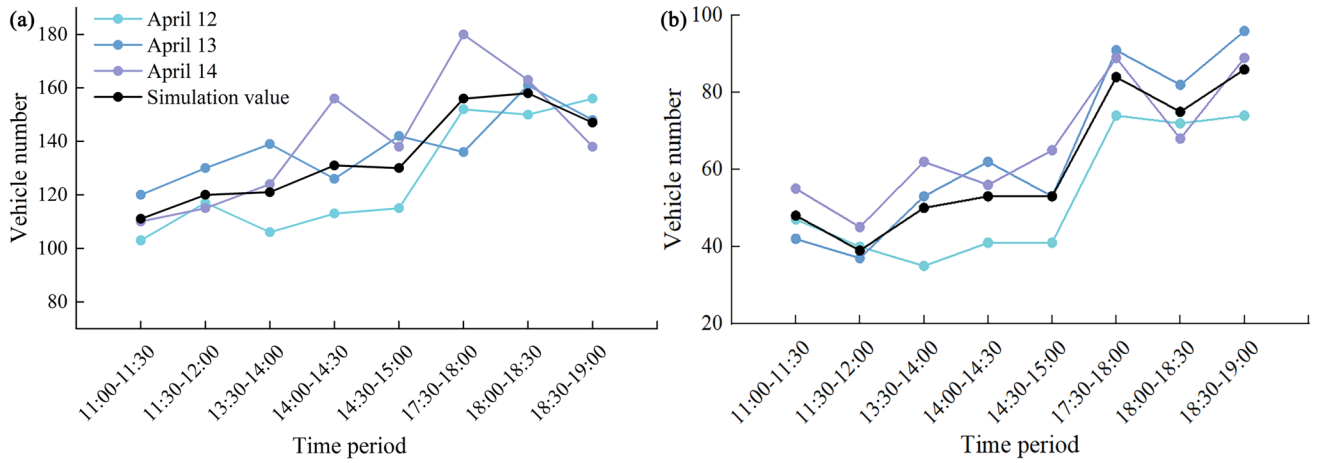

Fig. 4 Comparison of simulated and monitored values of traffic flow in both directions on Beigang Village Street. **a** Westbound, and **b** Eastbound

for given origin–destination (O–D) pairs and providing trip distance and duration data. We randomly selected 1726 O–D pairs and obtained trip distance and duration data from both Gaode Maps and the SUMO model. We then assessed the accuracy of the SUMO model using these data (Fig. 5). For trip distance, the goodness-of-fit (R^2) reaches 0.98, indicating that the constructed road network of Xiaoguwei Island in SUMO closely matches actual conditions depicted by Gaode Maps. For trip duration, R^2 is 0.69. Trip duration is inherently more challenging to simulate due to the complexity of real-world traffic participants, such as pedestrians and non-motorized vehicles, which can appear unpredictably. Although the trip duration results are not as strong as the trip distance results in terms of goodness-of-fit, the average trip duration under Gaode's real-time conditions is 473 s, while the SUMO simulation average is 463 s, indicating close agreement. Therefore, we conclude that the constructed SUMO model is suitable for traffic simulations on Xiaoguwei Island.

2.4 Integration of Flood and Traffic Models

The relationship between water depth and vehicle speed serves as the key link that integrates the flood model with the traffic model. We extracted water-depth time series from the triangular mesh elements corresponding to the

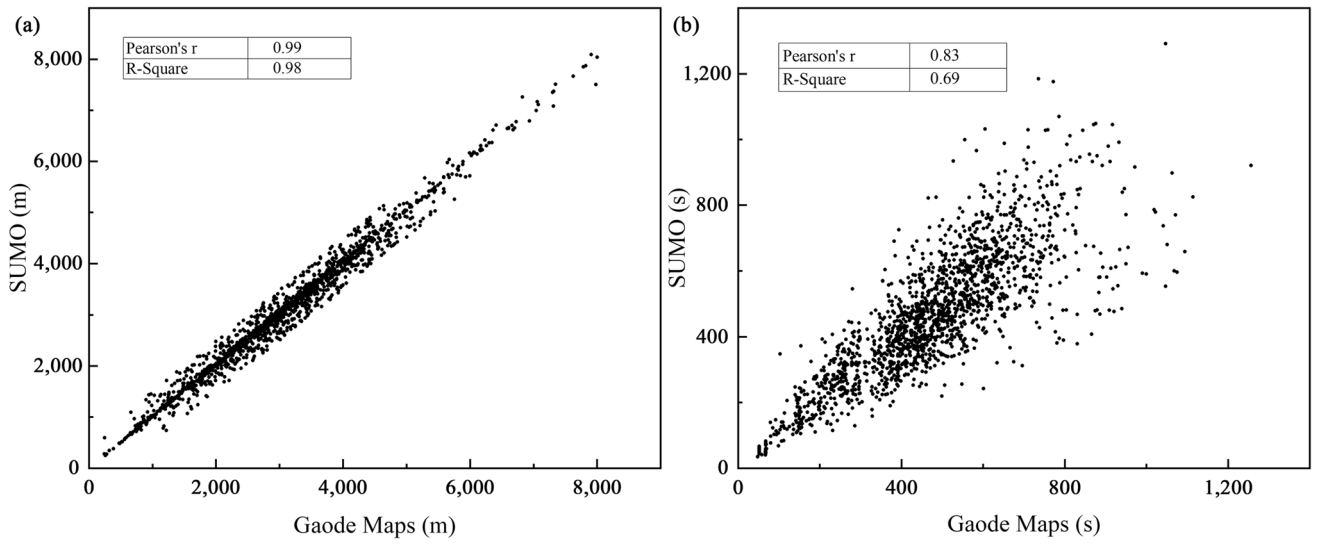

Fig. 5 Comparison of trip distance and trip duration between the Simulation of Urban Mobility (SUMO) model and Gaode Maps. **a** Trip distance, and **b** Trip duration

road nodes in the SUMO model. The following equation, derived from a field survey at six flood-prone locations in Beijing, China, was used to adjust the speed restrictions for vehicle movement (Du and Yang 2012). Given the similarities in road materials and vehicle types between Guangzhou and Beijing, the adoption of this formula in the study area is justifiable.

$$v = \frac{v_0}{2}\tanh\left(\frac{-h+a}{b}\right) + \frac{v_0}{2}, \tag{6}$$

where v is the acceptable vehicle speed in flooding scenarios; v_0 is the posted speed limit, which for different roads should take different values; h is the depth of water; a is the middle value of the water depth that vehicles stop running at; and b is the elasticity coefficient of attenuation, generally varying in the range [3, 5]. A smaller b value indicates a more rapid speed of attenuation.

The relationship between water depth and acceptable speed is illustrated by Fig. 6 using the study area's characteristic road speed limits of 40 and 50 km/h. When water depth surpasses 7 cm, acceptable travel speed decreases. When water depth exceeds 20 cm, vehicle speed is restricted to less than 5 km/h. We propose temporarily closing roads with water depths above 20 cm, and those road closures were implemented in the model. For roads with water depths between 7 and 20 cm, adjustable speed signs were implemented in the model to represent dynamic changes in vehicle speed limits.

3 Results

The integrated flood–traffic model was used to simulate regional traffic responses under rainstorms with different return periods. The design rainstorm scenarios started at 7:30 a.m. and ended at 9:30 a.m. To enhance the robustness, we began the simulation 1 h before the onset of rain. Due to the time lag between precipitation and surface runoff, we designated 12:00 p.m. as the end of the simulation to allow adequate time for surface water to drain back into the pipeline. Based on the results of the integrated model, we assessed the flood-prone areas and their inundation severity within the study area. The traffic efficiency of the region was systematically evaluated. Furthermore, we examined the accessibility of emergency vehicles, including those used by medical, fire, and public safety services, during rainstorms.

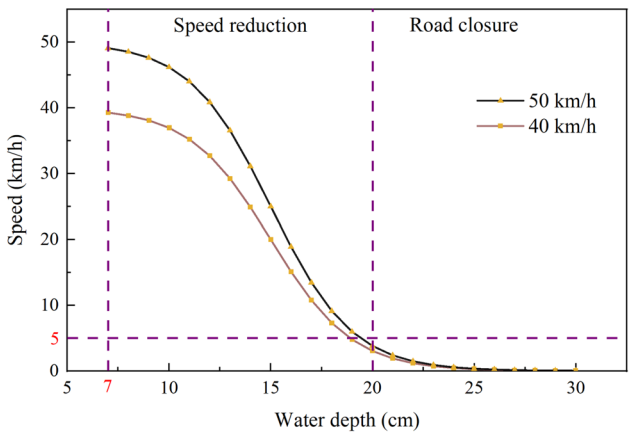

Fig. 6 Relationships between acceptable speed and water depth for roadways with two different speed limits: 40 km/h and 50 km/h

3.1 Inundation Analysis

The IHUM is capable of simulating water-depth variations for each mesh element, accurately capturing the spatial and temporal dynamics of the flood inundation process. To highlight the region's flood-prone areas, we focused on the maximum water depth of each mesh element throughout the simulation period and illustrated inundation based on varying return periods (Fig. 7). This mapping method is not time-specific. It evaluates the inundation performance of each mesh element over the entire rainstorm, visually pinpointing areas susceptible to flooding.

Figure 7 shows that as return periods increase, the scattered inundation under the 2-year rainfall event expands into deeper and more extensive flooding under the 100-year event. By comparing the simulated inundation distribution with topographic features visible in Google Earth imagery, we found that the vast majority of predicted inundation areas coincide with geomorphologically low-lying zones, which are naturally prone to water accumulation. This spatial coherence between the simulated flood extent and actual terrain depressions provides indirect yet meaningful evidence supporting the plausibility of the model results. Based on the flood simulation, under the 100-year rainfall event, 23.7% of the road segments in the study area would experience inundation depths of 20 cm or greater, indicating a substantial risk of road closure.

3.2 Characterization of the Response of the Overall Traffic System to Floods

Throughout the simulation period from 6:30 a.m. to 12:00 p.m., we calculated 15,500 O–D pairs in average travel time, average travel speed, and average lost time under various rainstorm scenarios, along with their variations compared to a sunny day (Table 3). The average lost time represents the duration of time lost due to reductions below optimal speed, including delays caused by factors such as waiting

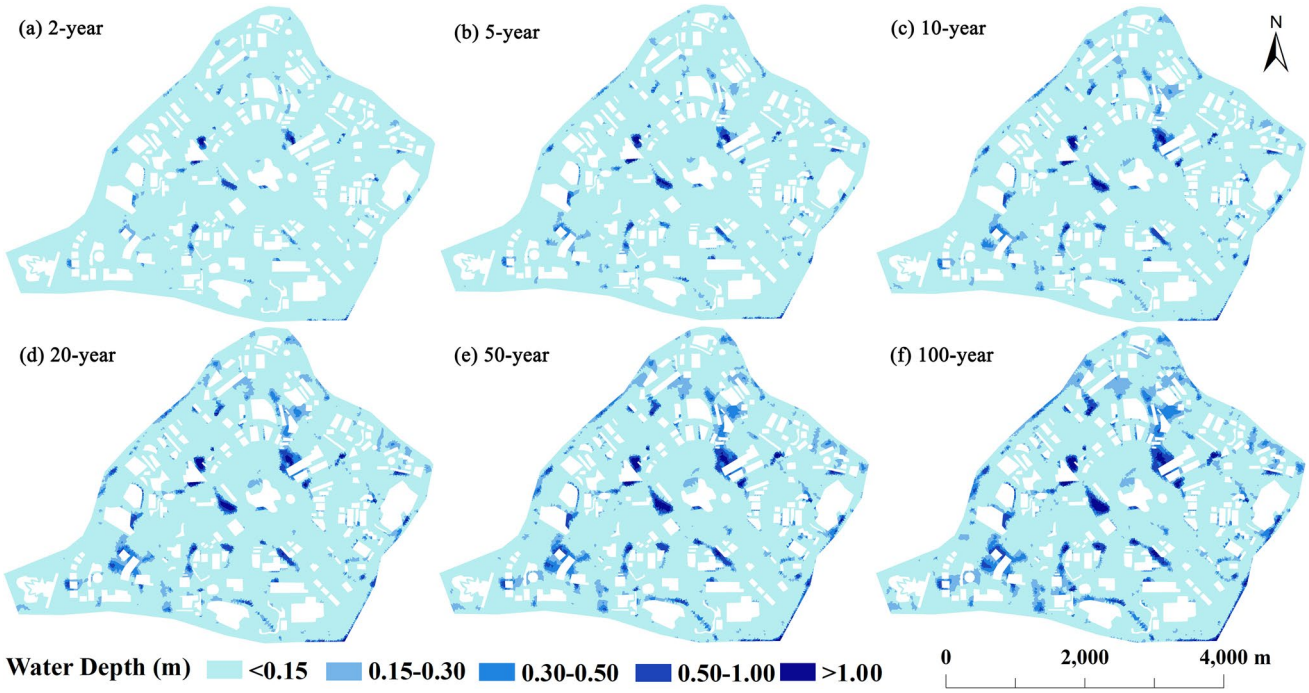

Fig. 7 Distribution of maximum inundation water depths for six rainstorms of different return periods on Xiaoguwei Island

Table 3 Overall origin–destination (O–D) pairs' trip assessment for the study area

Rainstorm event	Average travel time (s)	Increase (%)	Average travel speed (km/h)	Reduction (%)	Average lost time (s)	Increase (%)
Sunny	451	–	28	–	107	–
2-Year	601	33	22	21	232	117
5-Year	676	50	19	32	286	167
10-Year	732	62	18	36	325	204
20-Year	844	87	16	43	416	289
50-Year	940	108	14	50	484	352
100-Year	991	120	13	54	499	366

for a green light and deceleration resulting from wet road conditions.

Table 3 shows that the average travel speed on a sunny day is 28 km/h, consistent with statistics reported by the Guangzhou Transportation Bureau. As the intensity of the rainstorm increases, both average travel time and average lost time rise. During a 100-year return period rainstorm, the average travel time is 2.2 times longer than that on a sunny day, and the average lost time increases by 366%. Meanwhile, the average travel speed declines by 54%, from 28 to 13 km/h.

The accumulation of floodwater on roadways significantly impacts traffic flow, resulting in a notable decrease in overall traffic efficiency. At the same time, road closures alter the topology of the road network. Drivers reroute to roads with lower water levels, thereby concentrating more traffic on the remaining segments. This causes severe localized congestion or even traffic paralysis. Figure 8 presents the time series of average vehicle speeds during rainfall events across different return periods.

According to Fig. 8, following the onset of rainfall at 7:30 a.m., regional traffic speed gradually declines, with the speed reduction becoming more pronounced as the rainstorm's intensity increases. The rainstorm peaks at 8:20 a.m., typically followed by the peak runoff. The lowest vehicle speeds are influenced by the peak runoff and occur after it, indicating that the impact of the rainstorm on traffic is both prolonged and subject to a noticeable lag effect. As water gradually recedes, traffic conditions steadily improve. Figure 8 shows that a 2-h rainstorm with a two-year return

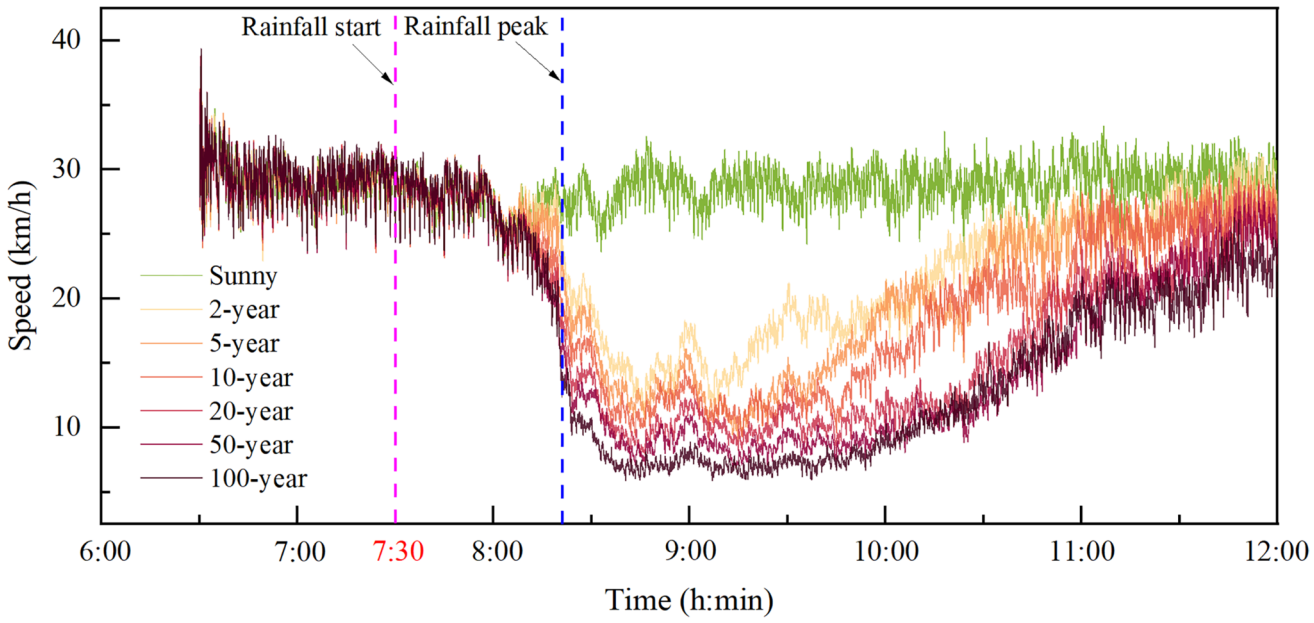

Fig. 8 Average vehicle speeds during rainfall events with different return periods

period impacts the study area for approximately 4.5 h. The rainstorm begins at 7:30 a.m., causing a continuous decline in traffic speeds until around 12:00 p.m., when speeds return to normal levels observed on a sunny day. Notably, a 100-year return period rainstorm has a much more prolonged impact on traffic efficiency.

3.3 Changes in Emergency Vehicle Mobility

A total of 42 traffic subdistricts were delineated based on the distribution of various universities and reserved villages on Xiaoguwei Island. The average area of each subdistrict is approximately 0.38 km^2. Xiaoguwei Island has 1 hospital, 1 fire station, and 10 police stations. The assumptions regarding emergency response are as follows: (1) all traffic subdistricts have the potential for incidents and require assistance from relevant emergency services. (2) The probability of an incident occurring in each subdistrict is proportional to its area. (3) We correspondingly raised the probability of a police vehicle responding to an accident due to the large number of police stations in the research area. (4) Ambulances, fire engines, and police vehicles are granted special driving privileges, including using the opposite direction lane for overtaking. (5) Emergency vehicles are allowed to drive at 120% of the road speed limit. Based on these assumptions, we established an O–D matrix using the hospital, fire station, and police stations as origins, and the 42 traffic subdistricts as destinations. During the simulation period from 6:30 a.m. to 12:00 p.m., a total of 177 emergency response trips were simulated, including 38 medical responses, 42 firefighting operations, and 97 police dispatches. Table 4 presents statistics on the mobility of emergency vehicles, including ambulances, fire engines, and police cars, under different rainstorm scenarios.

Table 4 illustrates that as both the volume and intensity of rainfall increase, the average travel time for emergency operations conducted by the medical, fire, and public safety services also rises. Correspondingly, the average travel speed of these emergency vehicles decreases significantly, with a reduction of more than 56%. In the public safety sector, the average response time increases from 4.83 min on a sunny day to 14.52 min during a 100-year return period rainstorm, while the average vehicle speed drops from 38.27 to 13.38 km/h. Roadway inundation caused by rainstorms disrupts the normal transportation function of roads, thereby impeding timely access to emergency services.

To illustrate the detouring behavior caused by flooding, we analyzed the differences in ambulance travel routes between identical origin and destination points both on a sunny day and under a 100-year return period rainstorm, using Dijkstra's algorithm embedded in the SUMO model. The Red Cross represents the hospital on Xiaoguwei Island, while Arabic numbers indicate residential points in need of medical services. We selected 21 residential points for route comparison (Fig. 9), with ambulance routes from the hospital to each location displayed in distinct colors. The ambulance routes to the same residential points during a sunny day and a 100-year return period rainstorm are depicted using the same colors.

As shown in Fig. 9, the 100-year return period rainstorm causes flooding on certain roads, blocking access and

Table 4 Statistics on the mobility of emergency vehicles across different rainstorm scenarios (speed factor = 1.20)

Event	Ambulances				Fire Engines				Police Cars			
	Average travel time (min)	Increase (%)	Average travel speed (km/h)	Reduction (%)	Average travel time (min)	Increase (%)	Average travel speed (km/h)	Reduction (%)	Average travel time (min)	Increase (%)	Average travel speed (km/h)	Reduction (%)
Sunny	4.25	–	37.06	–	4.39	–	37.46	–	4.83	–	38.27	–
2-Year	5.93	39.53	27.84	24.88	5.43	23.69	31.82	15.06	6.63	37.27	29.04	24.12
5-Year	5.50	29.41	30.56	17.54	5.42	23.46	32.77	12.52	7.96	64.80	24.73	35.38
10-Year	5.84	37.41	29.06	21.59	6.77	54.21	26.36	29.63	9.92	105.38	20.34	46.85
20-Year	6.74	58.59	26.05	29.71	7.57	72.44	24.27	35.21	11.05	128.78	18.04	52.86
50-Year	7.27	71.06	24.45	34.03	7.58	72.67	24.00	35.93	11.80	144.31	16.96	55.68
100-Year	10.08	137.18	16.26	56.13	11.16	154.21	15.47	58.70	14.52	200.62	13.38	65.04

making routes that are normally taken on a sunny day either more time-consuming to travel or impassable. Routes to the same destinations need to be changed, especially for residential points 1, 2, 17, and 19. For example, severe flooding at points A and B makes the usual routes to locations 1 and 17 impractical, requiring detours to provide medical care for residents, which increases travel time and puts residents' lives at risk.

4 Discussion

This study focused on evaluating the impacts of flooding on urban traffic. By adopting a water depth threshold of 20 cm, above which roads are closed for traffic, our results indicate that 23.7% of roads on Xiaoguwei Island experiences closures during a 100-year return period rainstorm. Similar findings were reported by Arrighi et al. (2019) in their study of Galluzzo in Florence, Italy, where 22.5% of roads became impassable under the most severe flooding scenario. More seriously, Singh et al. (2018) indicated that a 100-year return period rainstorm in Bangalore could lead to over 40% of roads experiencing disruption. These findings highlight the global prevalence of traffic disruptions caused by urban flooding, which pose significant threats to public safety, economic activity, and overall quality of life (Moles et al. 2021).

4.1 Road Closure Threshold and Water Depth–Vehicle Speed Relationship

During the dynamic progression of urban flooding, road water depth remains the primary factor affecting traffic operations (He et al. 2023). Road closures become necessary when vehicles can no longer navigate areas with significant water accumulation. Previous studies have adopted various road closure thresholds for passenger vehicles, including 20.3 cm (Miller 2022) and 30 cm (Kramer et al. 2016; Pregnolato et al. 2017; Li et al. 2018). For emergency vehicles, thresholds have been set at 25 cm (Green et al. 2017), 30 cm (Zhang et al. 2022), 50 cm (Zhang et al. 2022), and 60 cm (Kramer et al. 2016). In practice, research shows that as little as 15 cm of water can cause a passenger vehicle to lose control or stall (Pearson and Hamilton 2014), while depths of 20 cm may result in fatal accidents (Ahmed et al. 2020b). Moreover, based on the relationship between acceptable speed and water depth applied in this study, a depth of 20 cm corresponds to an acceptable driving speed of less than 5 km/h, indicating near-stall operating conditions. On this basis, our study adopted 20 cm as a road closure threshold for all vehicles.

In addition to conducting on-site observations in China to establish the water depth–vehicle speed relationship, some

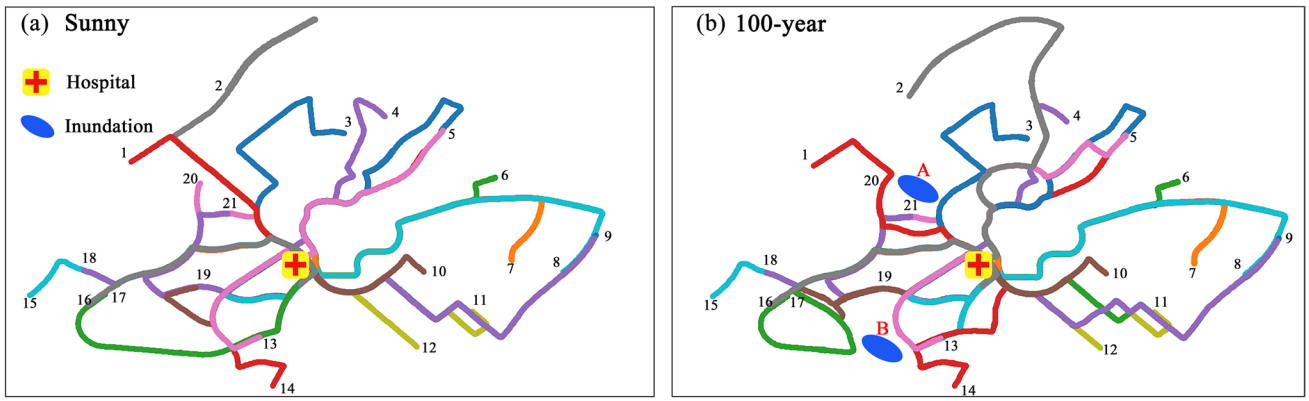

Fig. 9 Comparison of ambulance routes on a sunny day and under a 100-year return period rainstorm

researchers have integrated multi-source data, including experimental reports, expert opinions, and automobile driving videos from the United Kingdom and the United States (Pregnolato et al. 2016), observational data from Japan (Liu et al. 2016; Liu et al. 2020), and psychological questionnaire results from drivers (Su et al. 2016; Phanse et al. 2022) to explore this correlation. Choo et al. (2020) synthesized data from vehicles of various sizes (small, large, and four-wheel drive) to establish a generalized vehicle speed–depth curve. Currently, no consensus has been reached. At a water depth of 10 cm, the safe vehicle speed in this study is 36.96 km/h, while the questionnaire responses report 37.98 km/h and 37.50 km/h, respectively (excluding visibility factors). Other published curves suggest speeds ranging from 20.00 to 35.00 km/h. This indicates that, under low-water conditions, the depth–speed relationship adopted in this study reasonably captures drivers' general perceptions and observed operating characteristics. At a water depth of 20 cm, a vehicle's safe speed in this study drops below 5 km/h, compared to 32.28 km/h and 26.20 km/h from questionnaire responses, and 8 to 15 km/h from other curve estimates. This suggests that perception-based survey methods tend to overestimate vehicle passability under high-water conditions, whereas experimental, accident-oriented, and field observation-based studies place greater emphasis on the potential risk of loss of control.

4.2 Uncertainty Analysis of Emergency Vehicle Speed Factor

High-speed driving is a typical characteristic of emergency vehicles (Zhang et al. 2016; Hsiao et al. 2018), while their operating speeds often vary with road network density and population size (Lupa et al. 2021). An empirical study from Finland's Pirkanmaa Hospital District found that, on roads with speed limits of 40 km/h and 50 km/h, the average travel speeds of ambulances ranged from 1.08 to 1.35 times the posted limits under both normal and adverse weather conditions (Pappinen and Nordquist 2022). However, high-speed driving is closely associated with high crash rates and increased crash severity (Donoughe et al. 2012; Hsiao et al. 2018). Research indicates that the accident risk for emergency vehicle operators remains relatively manageable when speeds exceed the posted limit by no more than 10 mph (16.09 km/h) (Bui et al. 2018; Boland et al. 2023).

Based on this, we conducted an uncertainty analysis of emergency vehicles on Xiaoguwei Island, allowing them to operate at the maximum safety-limited speed of 135% of the posted limits. The results were compared with those obtained under the 120% speed limit assumption, which shows that the variation trends in average travel time and average travel speed across all rainstorm scenarios remain consistent, with slight numerical differences. For example, under a 100-year return period rainstorm, the 135% speed limit scenario resulted in a 48.15–67.70% decrease in average travel speed and a 1.10–2.36 times increase in average travel time relative to a sunny day. Similarly, under the 120% speed limit scenario, the corresponding values were 56.13–65.04% and 1.37–2.01 times, respectively. This indicates that rainstorms have largely consistent impacts on emergency vehicles, regardless of their operational speed. The observed low sensitivity of average travel time increases and average travel speed reductions to the speed factor parameter settings confirms the robustness of our findings across various hypothetical speed conditions.

4.3 Generalization and Policy Implications

The dynamic simulation framework proposed in this study holds significant potential for extension to other cities worldwide. However, its widespread application still faces several challenges. The first challenge concerns data availability, including terrain, drainage network, land use data, measured flood and traffic flow data, and socioeconomic information,

all of which are required for constructing and validating the integrated model. Second, the model parameters' transferability also poses some challenge. To account for variations in drainage conditions, road infrastructure, and population characteristics across cities, key parameters must be locally calibrated and adjusted. This includes determining modeling parameters within the flood and traffic models and defining locally relevant water depth–vehicle speed relationships. Successfully addressing these challenges is the key to ensuring the robust application of the framework worldwide.

This study offers valuable policy insights for urban flood mitigation and disaster risk reduction. Local authorities and transportation departments can integrate this dynamic simulation framework into municipal digital platforms, such as urban flood early warning systems and traffic management centers. This integration can help with flood risk assessment, road-section interruption duration prediction, and traffic response strategy development. The strategies may include modifying traffic signal timings to optimize the capacity of alternative routes; designating and safeguarding lifeline corridors for emergency vehicles, such as fire and medical services; and providing the public with real-time travel risk alerts and dynamic routing recommendations via mobile applications, roadside information displays, and navigation platforms (Niloy and Fries 2024; Haroon et al. 2025; Wu et al. 2025). For example, when flooding occurs on specific road segments, the system can draw on simulation results to identify available higher-elevation or better-drained detour corridors and push optimal safe routes to navigation terminals, thereby reducing vehicle stranding and preventing secondary incidents. In addition, authorities and stakeholders can evaluate the potential benefits of engineering interventions such as distributed sponge-city measures (Wang et al. 2023), localized drainage upgrades, roadway elevation improvements, and temporary pump deployment with the help of simulation outputs. Instead of relying solely on large-scale flood-control infrastructure, investment strategies should prioritize enhancing drainage and accessibility for critical corridors and network hubs. Overall, these insights suggest a closer integration of flood management, transportation planning, and emergency response, ultimately fostering flood-resilient, sustainable cities.

4.4 Limitations and Future Research

Integrated model validation remains a key research challenge in flood–traffic modeling due to data limitations. While efforts have been made to validate the flood and traffic models separately, few attempts have been made to validate the integrated flood–traffic model under varying conditions, including rainstorm events. Regarding urban flood modeling, a full model validation can rarely be achieved due to the lack of measured water depth data during flooding. In this study, we incorporated parameter sensitivity analysis, focusing on calibrating sensitive parameters to ensure the model's runoff aligns with the land-use characteristics of the study area. While the traffic model was validated using field survey data from key road sections and network-wide trip characteristics, this validation was performed exclusively under clear weather conditions. Therefore, we cannot definitively conclude that the developed traffic model fully reflects the actual traffic conditions of the study area under rainstorm scenarios. A promising avenue for future research is to integrate crowdsourcing or artificial intelligence technologies (for example, computer vision techniques and large language models) to collect water depth, inundation extent, and traffic flow data (Re et al. 2022; Lyu et al. 2025; Mohd Nazri et al. 2025), thereby strengthening the validation of flood–traffic models.

Three limitations in this study are further explained below. First, the model's analysis is based on a limited sample of 177 simulated emergency vehicle trips, which may compromise the overall reliability of the results. Accordingly, we conducted an uncertainty analysis on the speeding behavior of emergency vehicles. The results show that the impact of rainstorms is consistent across different driving speeds, which to some extent reduces the potential evaluation bias arising from a small sample size. Second, this study focused exclusively on passenger cars and emergency vehicles, excluding public transport, pedestrians, and non-motorized vehicles. Given that public transport, much like emergency vehicles, is a critical component for mitigating flood impacts and enhancing transportation system resilience (Alabbad and Demir 2025), the disruption of public transport service reliability during rainstorm events is also a topic worthy of exploration. Additionally, formulating strategies to guide pedestrians from flooded areas to shelters could provide valuable suggestions for more holistic urban flooding response planning (Musolino et al. 2022). Third, the framework adopts a uniform flood threshold for road closures, which does not differentiate between passenger cars and emergency vehicles. In reality, emergency vehicles often possess superior wading capabilities. Establishing vehicle type-specific closure thresholds and operational speed limits would further enhance the framework's practical utility.

5 Conclusion

This study proposed a novel dynamic flood–response simulation framework for urban transportation, designed to assess the impacts of varying intensity rainstorms and flooding on traffic systems. The key findings are as follows: (1) the proposed simulation framework effectively captures the dynamic impacts of rainstorms on regional transportation networks, providing a reliable method for urban flood–traffic

management. (2) A 100-year return period rainstorm significantly disrupts traffic flow, reducing average travel speed by 54%. (3) The effects of a 2-year return period rainstorm persist for more than 4.5 h, and the duration of traffic recovery increases with the rainstorm return period. (4) Road closures caused by inundation greatly impact vehicle mobility, particularly for emergency services.

Acknowledgments This study was supported by the National Natural Science Foundation of China (Grant No. 52279015), the State Key Laboratory of Subtropical Building and Urban Science (Grant No. 2023ZA01), the Department of Education of Guangdong Province, and the UK–China Institutional Partnership Exploration Fund by the British Council (Grant No. 6).

References

Ahmed, M.A., K. Haynes, and M. Taylor. 2020a. Vehicle-related flood fatalities in Australia, 2001–2017. *Journal of Flood Risk Management* 13(3): Article e2616.

Ahmed, M.A., K. Haynes, M. Tofa, G. Hope, and M. Taylor. 2020b. Duty or safety? Exploring emergency service personnel's perceptions of risk and decision-making when driving through floodwater. *Progress in Disaster Science* 5: Article 100068.

Alabbad, Y., and I. Demir. 2025. Understanding flood risk in public transit systems: Insights from accessibility and vulnerability analysis in Iowa. *International Journal of Disaster Risk Reduction* 126: Article 105615.

Arrighi, C., M. Pregnolato, R.J. Dawson, and F. Castelli. 2019. Preparedness against mobility disruption by floods. *Science of the Total Environment* 654: 1010–1022.

Boland, L.L., M.W. LeVoir, D. Jin, J.L. Duren, S.S. Souchtchenko, and A.C. Stevens. 2023. A retrospective, single-agency analysis of ambulance crashes during a 3-year period: Association with EMS driver characteristics and a telematics-measured safe driving score. *Prehospital Emergency Care* 27(4): 455–464.

Borowska-Stefańska, M., M. Kowalski, and S. Wiśniewski. 2019. The measurement of mobility-based accessibility—The impact of floods on trips of various length and motivation. *ISPRS International Journal of Geo-Information* 8(12): Article 534.

Bui, D.P., C. Hu, A.M. Jung, K.M. Pollack Porter, and S.C. Griffin. 2018. Driving behaviors associated with emergency service vehicle crashes in the U.S. Fire Service. *Traffic Injury Prevention* 19(8): 849–855.

Chakraborty, O., A. Das, A. Dasgupta, P. Mitra, S.K. Ghosh, and T. Mazumder. 2018. A multi-objective framework for analysis of road network vulnerability for relief facility location during flood hazards: A case study of relief location analysis in Bankura District, India. *Transactions in GIS* 22(5): 1064–1082.

Chang, H., M. Lafrenz, I.-W. Jung, M. Figliozzi, D. Platman, and C. Pederson. 2010. Potential impacts of climate change on flood-induced travel disruptions: A case study of Portland, Oregon, USA. *Annals of the Association of American Geographers* 100(4): 938–952.

Chen, W., G. Huang, H. Zhang, and W. Wang. 2018. Urban inundation response to rainstorm patterns with a coupled hydrodynamic model: A case study in Haidian Island, China. *Journal of Hydrology* 564: 1022–1035.

Choo, K.-S., D.-H. Kang, and B.-S. Kim. 2020. Impact assessment of urban flood on traffic disruption using rainfall–depth–vehicle speed relationship. *Water* 12(4): Article 926.

de Abreu, V.H.S., A.S. Santos, and T.G.M. Monteiro. 2022. Climate change impacts on the road transport infrastructure: A systematic review on adaptation measures. *Sustainability* 14(14): Article 8864.

Debionne, S., I. Ruin, S. Shabou, C. Lutoff, and J.-D. Creutin. 2016. Assessment of commuters' daily exposure to flash flooding over the roads of the Gard region, France. *Journal of Hydrology* 541: 636–648.

Donoughe, K., J. Whitestone, and H.C. Gabler. 2012. Analysis of firetruck crashes and associated firefighter injuries in the United States. *Annals of Advances in Automotive Medicine* 56: 69–76.

Du, L., and X. Yang. 2012. An exploration of influence of accumulated rainwater on urban traffic. In *ICCTP 2011: Towards sustainable transportation systems*, ed. Y. Yin, Y. Wang, J. Lu, and W. Wang, 187–198. Reston: American Society of Civil Engineers.

Fan, C., X. Jiang, and A. Mostafavi. 2021. Evaluating crisis perturbations on urban mobility using adaptive reinforcement learning. *Sustainable Cities and Society* 75: Article 103367.

Fan, C., X. Jiang, R. Lee, and A. Mostafavi. 2022. Equality of access and resilience in urban population–facility networks. *NPJ Urban Sustainability* 2(1): 1–12.

Gironás, J., L.A. Roesner, L.A. Rossman, and J. Davis. 2010. A new applications manual for the Storm Water Management Model (SWMM). *Environmental Modelling & Software* 25(6): 813–814.

Green, D., D. Yu, I. Pattison, R. Wilby, L. Bosher, R. Patel, P. Thompson, and K. Trowell et al. 2017. City-scale accessibility of emergency responders operating during flood events. *Natural Hazards and Earth System Sciences* 17(1): 1–16.

Hamzeie, R., P.T. Savolainen, and T.J. Gates. 2017. Driver speed selection and crash risk: Insights from the naturalistic driving study. *Journal of Safety Research* 63: 187–194.

Haroon, S.M., E. Smith, and A. Ryan. 2025. Optimizing sound alerts for traveler information systems: Insights from a driving simulator and eye tracking study. *Transportation Research Part F: Traffic Psychology and Behaviour* 114: 1077–1097.

He, H., R. Li, J. Pei, J.-P. Bilodeau, and G. Huang. 2023. Current overview of impact analysis and risk assessment of urban pluvial flood on road traffic. *Sustainable Cities and Society* 99: Article 104993.

Hsiao, H., J. Chang, and P. Simeonov. 2018. Preventing emergency vehicle crashes: Status and challenges of human factors issues. *Human Factors* 60(7): 1048–1072.

Jiang, L., Y. Chen, and H. Wang. 2015. Urban flood simulation based on the SWMM model. *Proceedings of IAHS* 368: 186–191.

Krajzewicz, D. 2010. Traffic simulation with SUMO—Simulation of urban mobility. In *Fundamentals of traffic simulation*, ed. J. Barceló, 269–293. New York: Springer.

Kramer, M., K. Terheiden, and S. Wieprecht. 2016. Safety criteria for the trafficability of inundated roads in urban floodings. *International Journal of Disaster Risk Reduction* 17: 77–84.

Li, M., Q. Huang, L. Wang, J. Yin, and J. Wang. 2018. Modeling the traffic disruption caused by pluvial flash flood on intra-urban road network. *Transactions in GIS* 22(1): 311–322.

Li, Y., J. Gong, L. Niu, and J. Sun. 2019. A physically based spatiotemporal method of analyzing flood impacts on urban road networks. *Natural Hazards* 97(1): 121–137.

Li, J., G. Huang, and W. Chen. 2024. Improvement of city rainfall model subcatchment structure based on urban hydrology process. *Journal of Hydrologic Engineering* 29(2): Article 05024001.

Li, J., J. Zeng, G. Huang, and W. Chen. 2024. Urban flood mitigation strategies with coupled gray-green measures: A case study in Guangzhou City, China. *International Journal of Disaster Risk Science* 15(3): 467–479.

Liu, M.-W., Y. Oeda, and T. Sumi. 2016. Modeling free-flow speed according to different water depths—From the viewpoint of dynamic hydraulic pressure. *Transportation Research Part D: Transport and Environment* 47: 13–21.

Liu, M., M. Chiaki, Y. Oeda, and T. Sumi. 2020. Modelling fundamental diagrams according to different water film depths from the perspective of the dynamic hydraulic pressure. *Scientific Reports* 10(1): Article 6496.

Lopez, P.A., M. Behrisch, L. Bieker-Walz, J. Erdmann, Y.-P. Flötteröd, R. Hilbrich, L. Lücken, J. Rummel, et al. 2018. Microscopic traffic simulation using SUMO. In *2018 21st International Conference on Intelligent Transportation Systems (ITSC)*, 4–7 November 2018, Maui, HI, USA, 2575–2582.

Lu, X., F.K. Shun Chan, W.-Q. Chen, H.K. Chan, and X. Gu. 2022. An overview of flood-induced transport disruptions on urban streets and roads in Chinese megacities: Lessons and future agendas. *Journal of Environmental Management* 321: Article 115991.

Lupa, M., M. Chuchro, W. Sarlej, and K. Adamek. 2021. Emergency ambulance speed characteristics: A case study of Lesser Poland voivodeship, southern Poland. *GeoInformatica* 25(4): 775–798.

Lutoff, C., J.-D. Creutin, I. Ruin, S. Duvillard, S. Anquetin, and M. Borga. 2018. Exposure to flash floods: The conflict between human mobility and water mobility. In *Mobility in the face of extreme hydrometeorological events 1*, ed. C. Lutoff, and S. Durand, 211–240. Amsterdam: Elsevier.

Lyu, H., S. Zhou, Z. Wang, G. Fu, and C. Zhang. 2025. Assessing large multimodal models for urban floodwater depth estimation. *Water Resources Research* 61(4): Article e2024WR039494.

Markolf, S.A., C. Hoehne, A. Fraser, M.V. Chester, and B.S. Underwood. 2019. Transportation resilience to climate change and extreme weather events—Beyond risk and robustness. *Transport Policy* 74: 174–186.

Martínez-Gomariz, E., M. Gómez, B. Russo, and S. Djordjević. 2018. Stability criteria for flooded vehicles: A state-of-the-art review. *Journal of Flood Risk Management* 11(S2): S817–S826.

Miller, R.L. 2022. Modeling temporal accessibility of an urban road network during an extreme pluvial flood event. *Natural Hazards Review* 23(4): Article 04022032.

Mohd Nazri, M.A., F. Samsuri, and V. Narayanamurthy. 2025. Design and analysis of visual vehicle tracking system for traffic surveillance using deep learning. *International Journal of Intelligent Transportation Systems Research* 23(1): 592–602.

Moles, A., T. Birch, Y.L. Chan, D. Yang, H. Zhu, and K.E. Cherry. 2021. Community vulnerabilities and wellbeing after disaster. In *The intersection of trauma and disaster behavioral health*, ed. K.E. Cherry, and A. Gibson, 247–269. Cham: Springer.

Musolino, G., R. Ahmadian, and J. Xia. 2022. Enhancing pedestrian evacuation routes during flood events. *Natural Hazards* 112(3): 1941–1965.

Niloy, M.T.A., and R.N. Fries. 2024. Actuated signal timing optimization for a no-notice evacuation with high left-turn demands. *Urban Science* 8(3): Article 85.

Paleari, L., E. Movedi, M. Zoli, A. Burato, I. Cecconi, J. Errahouly, E. Pecollo, and C. Sorvillo et al. 2021. Sensitivity analysis using Morris: Just screening or an effective ranking method?. *Ecological Modelling* 455: Article 109648.

Pappinen, J., and H. Nordquist. 2022. Driving speeds in urgent and non-urgent ambulance missions during normal and reduced winter speed limit periods—A descriptive study. *Nursing Reports* 12(1): 50–58.

Pearson, M., and K. Hamilton. 2014. Investigating driver willingness to drive through flooded waterways. *Accident Analysis & Prevention* 72: 382–390.

Phanse, S., M. Chaturvedi, and S. Srivastava. 2022. Modelling and simulation of road traffic under rainy conditions. In *2022 14th International Conference on COMmunication Systems & NETworkS (COMSNETS)*, 4–8 January 2022, Bangalore, India, 830–835.

Pregnolato, M., A. Ford, and R. Dawson. 2016. Disruption and adaptation of urban transport networks from flooding. *E3S Web of Conferences* 7: Article 07006.

Pregnolato, M., A. Ford, S.M. Wilkinson, and R.J. Dawson. 2017. The impact of flooding on road transport: A depth-disruption function. *Transportation Research Part D: Transport and Environment* 55: 67–81.

Pyatkova, K., A.S. Chen, S. Djordjević, D. Butler, Z. Vojinović, Y.A. Abebe, and M. Hammond. 2019. Flood impacts on road transportation using microscopic traffic modelling techniques. In *Simulating urban traffic scenarios*, ed. M. Behrisch, and M. Weber, 115–126. Cham: Springer.

Re, M., L.D. Kazimierski, P.E. Garcia, N.E. Ortiz, and M. Lagos. 2022. Assessment of crowdsourced social media data and numerical modelling as complementary tools for urban flood mitigation. *Hydrological Sciences Journal* 67(9): 1295–1308.

Rentschler, J., M. Salhab, and B.A. Jafino. 2022. Flood exposure and poverty in 188 countries. *Nature Communications* 13(1): Article 3527.

Shahdani, F.J., M. Santamaria-Ariza, H.S. Sousa, M. Coelho, and J.C. Matos. 2022. Assessing flood indirect impacts on road transport networks applying mesoscopic traffic modelling: The case study of Santarém, Portugal. *Applied Sciences* 12(6): Article 3076.

Singh, P., V.S.P. Sinha, A. Vijhani, and N. Pahuja. 2018. Vulnerability assessment of urban road network from urban flood. *International Journal of Disaster Risk Reduction* 28: 237–250.

Su, B., H. Huang, and Y. Li. 2016. Integrated simulation method for waterlogging and traffic congestion under urban rainstorms. *Natural Hazards* 81(1): 23–40.

Suarez, P., W. Anderson, V. Mahal, and T.R. Lakshmanan. 2005. Impacts of flooding and climate change on urban transportation: A systemwide performance assessment of the Boston Metro Area. *Transportation Research Part D: Transport and Environment* 10(3): 231–244.

Tang, J., P. Zhao, Z. Gong, H. Zhao, F. Huang, J. Li, Z. Chen, and L. Yu et al. 2023. Resilience patterns of human mobility in response to extreme urban floods. *National Science Review* 10(8): Article nwad097.

Tobin, D.M., M.R. Kumjian, and A.W. Black. 2021. Effects of precipitation type on crash relative risk estimates in Kansas. *Accident, Analysis and Prevention* 151: Article 105946.

Vajjarapu, H., A. Verma, and H. Allirani. 2020. Evaluating climate change adaptation policies for urban transportation in India. *International Journal of Disaster Risk Reduction* 47: Article 101528.

Wang, W., S. Yang, H.E. Stanley, and J. Gao. 2019. Local floods induce large-scale abrupt failures of road networks. *Nature Communications* 10(1): Article 2114.

Wang, W., S. Yang, J. Gao, F. Hu, W. Zhao, and H.E. Stanley. 2020. An integrated approach for assessing the impact of large-scale future floods on a highway transport system. *Risk Analysis* 40(9): 1780–1794.

Wang, Y., C. Zhang, A.S. Chen, G. Wang, and G. Fu. 2023. Exploring the relationship between urban flood risk and resilience at a

high-resolution grid cell scale. *Science of the Total Environment* 893: Article 164852.

Wu, J., Y. Lin, and W. Qi. 2025. Timing co-evolutionary path optimisation method for emergency vehicles considering the safe passage. *Transportmetrica A: Transport Science* 21(2): Article 2253477.

Zhang, Z., Q. He, J. Gou, and X. Li. 2016. Performance measure for reliable travel time of emergency vehicles. *Transportation Research Part C: Emerging Technologies* 65: 97–110.

Zhang, M., M. Xu, Z. Wang, and C. Lai. 2021. Assessment of the vulnerability of road networks to urban waterlogging based on a coupled hydrodynamic model. *Journal of Hydrology* 603: Article 127105.

Zhang, Y., X. Li, N. Kong, M. Zhou, and X. Zhou. 2022. Spatial accessibility assessment of emergency response of urban public services in the context of pluvial flooding scenarios: The case of Jiaozuo Urban Area, China. *Sustainability* 14(24): Article 16332.

Zheng, J., and G. Huang. 2023. A novel grid cell-based urban flood resilience metric considering water velocity and duration of system performance being impacted. *Journal of Hydrology* 617: Article 128911.

Zhu, X., Q. Dai, D. Han, L. Zhuo, S. Zhu, and S. Zhang. 2019. Modeling the high-resolution dynamic exposure to flooding in a city region. *Hydrology and Earth System Sciences* 23(8): 3353–3372.

Zou, Y., Y. Zhang, and K. Cheng. 2021. Exploring the impact of climate and extreme weather on fatal traffic accidents. *Sustainability* 13(1): Article 390.